Wang, Qiming; Sihvola, Ari; Qi, Jiaran

A Novel Procedure To Hybridize The Folded Transmitarray and Fabry Perot Cavity With Low Antenna Profile and Flexible Design Frequency

Published in:
IEEE Antennas and Wireless Propagation Letters

DOI:
10.1109/LAWP.2024.3398076

Published: 01/01/2024

Document Version
Peer-reviewed accepted author manuscript, also known as Final accepted manuscript or Post-print

Please cite the original version:
Wang, Q., Sihvola, A., & Qi, J. (2024). A Novel Procedure To Hybridize The Folded Transmitarray and Fabry Perot Cavity With Low Antenna Profile and Flexible Design Frequency. *IEEE Antennas and Wireless Propagation Letters*, *23*(8), 2501-2505. https://doi.org/10.1109/LAWP.2024.3398076

A Novel Procedure To Hybridize The Folded Transmitarray and Fabry Perot Cavity With Low Antenna Profile and Flexible Design Frequency

Qiming Wang, Ari Sihvola, *IEEE Life Fellow*, and Jiaran Qi, *IEEE Senior Member*

***Abstract*—The previously reported procedure to hybridize the high-band folded-transmitarray (FTA) and the low-band Fabry-Perot-cavity-antenna (FPCA) adopts the $\lambda_{low}/2$ FPCA as the basic antenna, the FTA is then integrated with the FPCA. The aperture size and profile of the implemented antenna are highly correlated to the λ_{low} which restricts further profile shrunk and designable λ_{low} under a given aperture size. A novel procedure tackling these issues is proposed. A double-folded FTA (DFFTA) whose profile is 1/4 of the focal length is first adopted as the basic antenna under a given aperture size. Then, an FPCA with an Artificial-Magnetic-Conductor (AMC) loaded ground is integrated with the DFFTA. The aperture size and the profile of the implemented antenna are completely determined by the DFFTA which has no correlations of the λ_{low}. An aperture-shared dual-band antenna with a lower profile at both operating bands can be designed by this procedure. Further, the λ_{low} can be freely chosen under a given aperture size and profile. An aperture-shared surface offering partial-reflection at 3.5 GHz and phase-correction at 28 GHz, and an aperture-shared multi-functional ground offering polarization conversion at 28 GHz and phase compensation at 3.5 GHz are proposed to execute the proposed procedure.**

***Index Terms*—Aperture-shared multi-band antenna, double-folded transmitarray, low-profile, Fabry Perot cavity, high gain.**

I. Introduction

APERTURE-SHARED multi-band high gain antennas have been extensively studied over the past few years for their better space reuse efficiency and the realized larger central frequency ratio [1]–[5]. The Sub-6 GHz and Millimeter-Wave (mm-wave) integrated 5G networks have been demonstrated to offer a consistent user experience and high-speed large-volume data transmission simultaneously [6]–[9]. The aperture-shared technique can be a better candidate to fulfill the front-end needs of the 5G communication links [10]. High-gain antennas with lower insertion loss such as transmitarray (TA), metalens, and Fabry-Perot-Cavity antenna (FPCA) [11]–[15] can be a better choice for performing aperture multiplexing due to their planar and easy integration properties.

This paper was partially supported by National Natural Science Foundation of China under Grant no. 62271170, and no. 61671178.

Q. Wang and J. Qi are with Microwave Engineering Dept., School of Electronics and Information Engineering, Harbin Institute of Technology, China (*Corresponding author: Jiaran Qi*, e-mail: qi.jiaran@hit.edu.cn).

Ari Sihvola is with the Department of Electronics and Nanoengineering, Aalto University, 00076 Espoo, Finland.

Aperture-shared antennas hybridizing a low-band FPCA and a high-band FZP lens [16] or folded TA (FTA) [17], [18] have been proposed. These antennas achieve high gain in both bands without any feeding networks. However, the strong correlations between the λ_{low} and the aperture size and profile of the antenna make their performance sub-optimized, especially as they lack the ability to be integrated into more space-constrained systems and the inflexible designable frequency at the lower band. This is mainly due to the inadequate hybridization procedure.

The reported construction procedure is depicted in Fig. 1(a) which adopts a $\lambda_{low}/2$ FPCA as the basic antenna under a given f_{low}. Next, the $F/2$ FTA is built under the same profile ($\lambda_{low}/2$) of the FPCA. The F is equal to the λ_{low}. Typically, the F/D of the TA is chosen around 0.5 for wider gain bandwidth and superior aperture efficiency [19]. The aperture size of the antenna can thus be calculated as $\lambda_{low}* D/F$ which equals $2\lambda_{low}$. According to this hybridization procedure, the aperture size and profile of the aperture-shared antenna are highly correlated to the λ_{low}. In [15]–[18], the antenna profiles are all around $\lambda_{low}/2$. In [15] and [17], the aperture sizes are all $\lambda_{low}* D/F$. In [16], the aperture size is $\lambda_{low}* D/2F$ since the profile of the FZP lens is F. In [18], a $F/3$ FTA is adopted, and the aperture size is thus $\lambda_{low}* 3D/2F$. The strong correlations restrict further profile shrunk which is necessary for integration into more space-constrained systems. Further, the designable λ_{low} is restricted under a given aperture size, although different D/F can alleviate this phenomenon, this will deteriorate the performance of the FTA [19], especially the realized gain bandwidth.

In this letter, a novel procedure to hybridize the FPCA and the FTA is proposed to implement a dual-band aperture-shared antenna with a lower profile and more flexible designable λ_{low}. Different from the reported, a double-folded FTA (DFFTA) is first designed under a given aperture size (D). The profile of the DFFTA can be calculated as $D/8$. Then, a shrunk FPCA with an AMC-loaded ground plane is designed under the same aperture size and profile of the DFFTA. The aperture size and profile of the aperture-shared antenna are fully determined by the DFFTA which do not correlate to the λ_{low}, the issues can thus be tackled.

II. Hybridization Procedure of The Antenna

The proposed hybridization procedure of the aperture-shared antenna is shown in Fig. 1(b). The proposed antenna adopts a

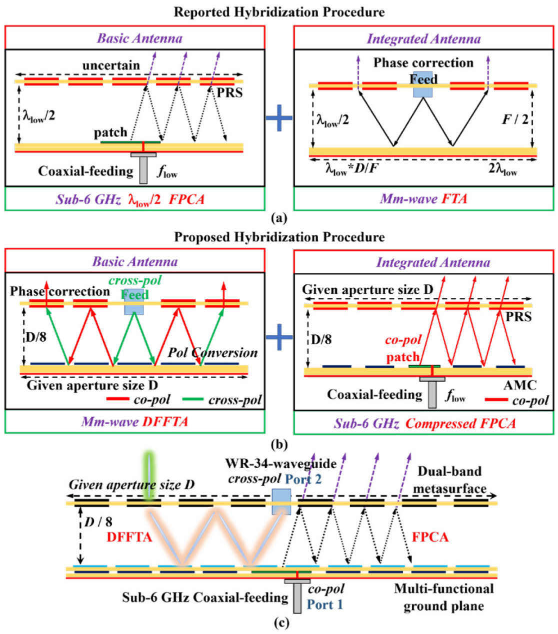

Fig. 1. (a) The reported hybridization procedure of the aperture-shared antenna [17]. (b) The proposed hybridization procedure of the aperture-shared antenna. (c) The schematic diagram of the proposed aperture-shared dual-band antenna.

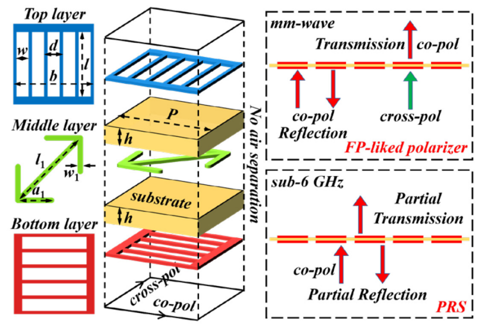

Fig. 2. Configuration of the proposed dual-band metasurface unit cell. (P = 6 mm, h = 1.5 mm, b = 5.8 mm, l = 4.8 mm, w = 0.9 mm, d = 1.3 mm, l_1 = 6 mm, w_1 = 0.4 mm)

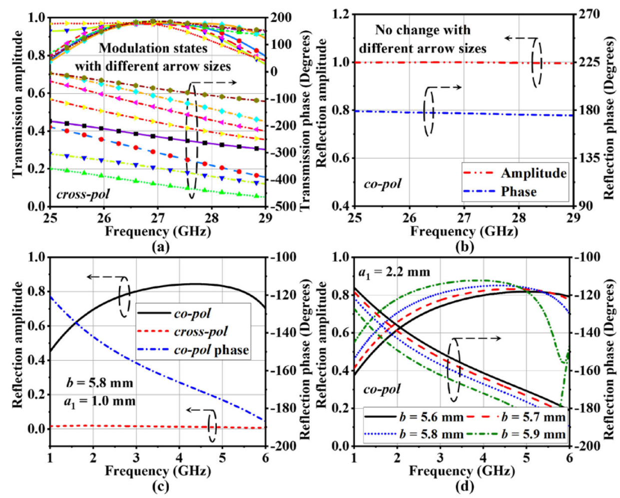

Fig. 3. (a) The simulated *cross-pol* transmission phase and amplitude of the unit cell at the mm-wave band. (b) The simulated *co-pol* reflection properties of the unit cell at the mm-wave band. (c) The simulated reflection properties at the sub 6 GHz band. (d) The simulated *co-pol* reflection properties of the unit cell at the sub-6 GHz band with different patch sizes.

DFFTA [20], [21] as the basic antenna under a given aperture size (D). The profile of the DFFTA equals F/4. The DFFTA is comprised of a phase correction metasurface and a polarization conversion ground plane. The feed is placed at the center of the upper metasurface and radiated *cross-pol* electromagnetic (EM) wave. The EM waves fulfill three specular reflections between the upper metasurface and the polarization conversion ground. The ground can twist the polarization states of the incident EM waves with 90°. The upper metasurface fully reflects the *co-pol* wave and passes through the *cross-pol* wave with polarization conversion and phase modulation. The F/D is chosen as 0.5 for higher aperture efficiency and wider gain bandwidth [19]. The profile of the DFFTA can be ascertained as D/8. Next, under an aperture size of D and an antenna profile of D/8, the sub-6 GHz FPCA is integrated into the same aperture with the same profile. Since the cavity height of the FPCA strongly correlates to the operating wavelength, to break this restriction, an AMC-loaded ground is used. The AMC can compensate for the propagation phase differences within a given cavity height (D/8) at different frequencies. The aperture-shared antenna thus gains a flexible designable frequency at the sub-6 GHz band.

By combining the DFFTA and the FPCA, an aperture-shared dual-band high-gain antenna can be constructed. The structure diagram of the antenna is shown in Fig. 1(c). As can be found, the proposed antenna consists of a dual-band upper metasurface, a multi-functional ground, a waveguide feed for the DFFTA, and a feeding patch for the FPCA. The dual-band metasurface requires to provide phase correction at the mm-wave band and partial reflection at the sub-6 GHz band. The multi-functional ground needs to provide polarization transition at the mm-wave band and phase compensation at the sub-6 GHz band.

III. MM-WAVE/SUB-6 GHZ ANTENNA IMPLEMENTATION

A. *Design of the dual-band metasurface unit cell*

To satisfy the requirements for hybridizing the DFFTA and the FPCA, a triple-layer compact dual-band unit cell illustrated in Fig. 2 is proposed. It consists of three metallic layers and two dielectric slabs. The material of the dielectric is F4B with a ε_r of 2.65 and a loss tangent of 0.003. The top layer and bottom layer of the unit cell are constructed by a square patch with five slots. The middle layer is a diagonally pointed double-headed arrow structure [19]. This unit cell can be regarded as an FP-liked [22] polarizer at the mm-wave band fully reflecting the *co-pol* EM waves and efficiently transmitting and modulating the phase of the *cross-pol* waves. The transmission phase can be adjusted by the diagonal orientation (45° or 135°) and length (a_1) of the arrow. At the sub-6 GHz band, the discrimination of the waves is reduced, and the anisotropic unit thus equals a quasi-isotropic unit offering partial reflection without polarization conversion.

The commercial software CST Microwave Studio is utilized to get the simulation results. The F-solver is adopted to simulate the unit cell applied with the periodic boundary conditions. The *cross-pol* transmission property at the mm-wave band is shown in Fig. 3(a). This unit exhibits a higher than 0.82 transmission amplitude and a nearly 360° transmission phase coverage. Fig. 3(b) illustrates the *co-pol* reflection phase and amplitude. It can be found that this unit fully reflects the *co-pol* EM waves under different arrow sizes. The oblique incidence analysis indicates that the transmission amplitude and transmission phase differ little within the incidence angle range of 0°–40°.

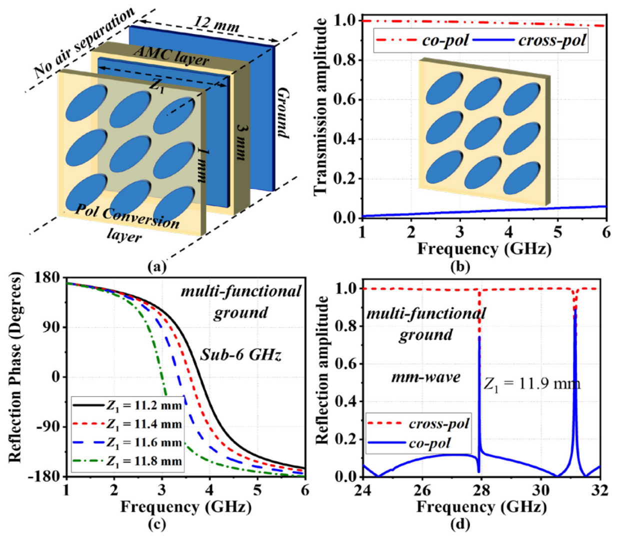

Fig. 4. (a) Configuration of the proposed multi-functional ground unit cell. (b) The simulated transmission property of the elliptical array. (c) The simulated reflection phase of the multi-functional unit cell at the sub-6 GHz band. (d) The simulated reflection amplitude of the unit cell at the mm-wave band.

Fig. 3(c) shows the reflection properties of the unit cell at the sub-6 GHz band. This unit cell exhibits a larger than 0.7 *co-pol* reflection amplitude within the band of 2–6 GHz. The *cross-pol* reflection amplitude is nearly zero in this range which indicates the quasi-isotropic properties of the unit at the sub-6 GHz band. Fig. 3(d) shows the simulated *co-pol* reflection amplitude under different patch sizes. The operating frequency at the sub-6 GHz band can be adjusted by varying the size of the patch (b). In the incidence angle range of 0°–60°, the amplitude remains larger than 0.8 in the frequency range of 3.0 GHz–5.5 GHz. At the same time, the fluctuation of the phase is less than 10°.

B. Design of the multi-functional ground unit cell

To construct the DFFTA, the ground plane needs to provide polarization conversion at the mm-wave band. To construct the FPCA with flexible design frequency under a given profile, the ground needs to compensate for the phase difference at the sub-6 GHz band. Here, a novel triple-layered multi-functional unit cell illustrated in Fig. 4(a) is proposed. This unit cell consists of an AMC layer [23]–[25], a polarization conversion elliptical patch layer, and a ground. The dielectric material is the same as the metasurface. The AMC provides phase compensation at the sub-6 GHz band and simultaneously serves as the ground of the elliptical patch array at the mm-wave band. Other types of AMC can also be utilized while requiring to provide equivalent ground for the elliptical patch array. The elliptical patch layer can realize reflection polarization conversion at the mm-wave band. The top loading of the elliptical array has little effect on the properties of the AMC since the elliptical array provides high *co-pol* transmission amplitude at the sub-6 GHz band (Fig. 4(b)). The reflection performance of the multi-functional unit at the sub-6 GHz band and mm-wave band are shown in Fig. 4(c) and Fig. 4(d), respectively. The low-band reflection phase can be modulated by changing the size of the AMC patch (Z_1). The fluctuation of the reflection phase is less than 60° within the incident angle range of 0°–40°. Few parasitic resonances occur at the mm-wave band which is due to the incomplete equivalent ground (AMC patch). These resonances are narrowband. Apart

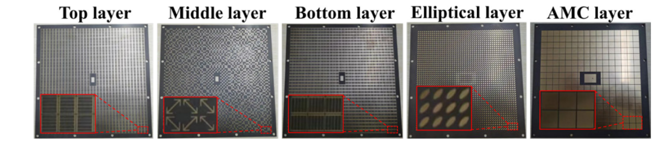

Fig. 5. The fabricated aperture-shared dual-band antenna prototype.

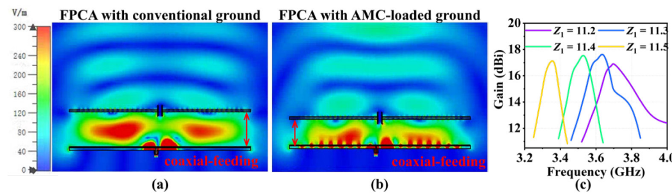

Fig. 6. (a) The simulated E-field of the FPCA with conventional ground and (b) AMC-loaded ground. (c) The simulated gain of the aperture-shared antenna at the sub-6 GHz band with different AMC patch sizes (Z_1).

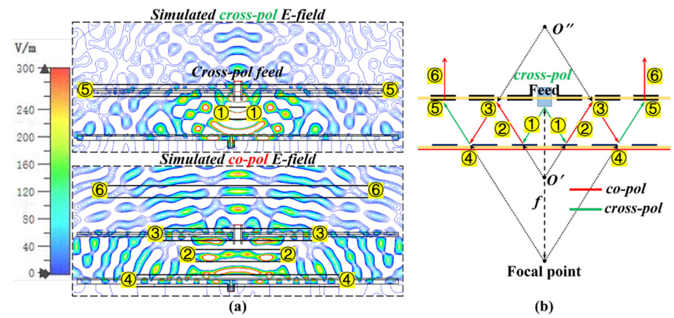

Fig. 7. (a) The simulated E-field of the DFFTA at 27 GHz. (b) The path folding mechanism of the mm-wave DFFTA.

from these resonances, the reflection amplitude is higher than 0.99 from 24.0 GHz to 33.0 GHz. The *cross-pol* reflection amplitude is around 0.7 when the incidence angle reaches 60°.

IV. Antenna Measurement and Discussion

A. Prototype fabrication and antenna measurement

The proposed dual-band antenna is fabricated and measured in the anechoic chamber, as shown in Fig. 5. The aperture size is configured as 220 mm × 220 mm which is about $2.6\lambda_{low}$. The upper metasurface contains 34 × 34 unit cells. To integrate the WR-34 waveguide, a 2 × 4 array of the unit cells at the center of the upper metasurface is deleted. The waveguide outstretches into the FP cavity with 4.0 mm to decrease the mutual coupling from the adjacent unit cells. The F/D of the DFFTA is chosen as 0.5 to balance the aperture efficiency and the gain bandwidth [19]. The F of the DFFTA is 110 mm. After quarter-folded, the profile of the cavity can be ascertained as (110 + 4)/4 = 28.5 mm which is only $0.33\lambda_{low}$ (3.5 GHz). The profile-to-diameter ratio of the proposed antenna is only 0.13 which is the smallest value compared with the reported FPCA–FTA configuration. A coaxial-feeding patch with a size of 22.5 mm × 16.8 mm is used as the low band feed. A standard WR-34 waveguide is adopted as the feed of DFFTA. A server with 256 GB RAM is used to finish the simulations. The antenna is simulated by the T-solver in CST and the single simulation time is around 60 hours.

The simulated E-field of the FPCA with conventional ground and AMC-loaded ground is shown in Fig. 6. Strong E-field on the AMC ground (Fig. 6(b)) and both quasi-plane emitted fields from the aperture verified the efficient phase compensation of the AMC for shrinking the profile. Under the same aperture size

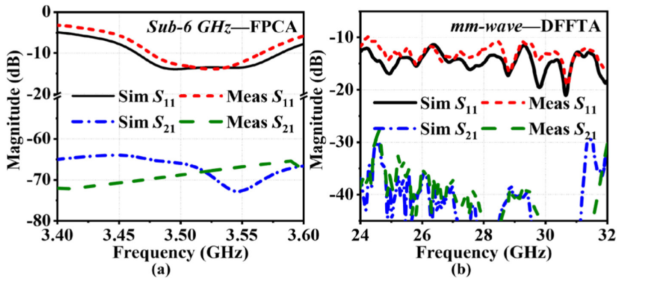

Fig. 8. (a) The simulated and measured S_{11} of the proposed antenna at the sub-6 GHz band and (b) at the mm-wave band.

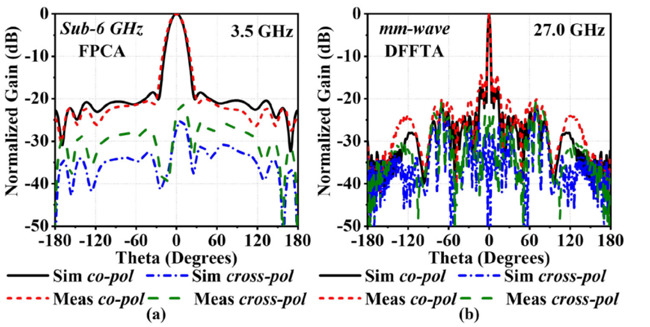

Fig. 9. (a) The normalized radiation pattern of the proposed antenna at the sub-6 GHz band (3.5 GHz) and (b) at the mm-wave band (27.0 GHz).

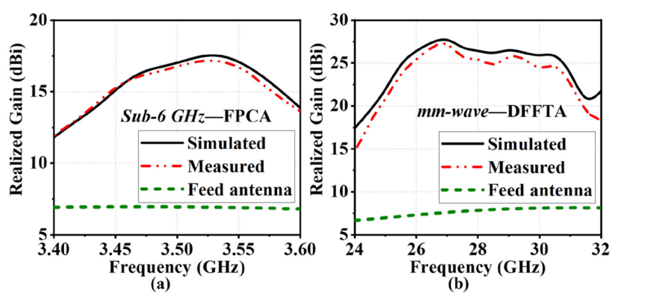

Fig. 10. (a) The simulated and measured gain of the proposed antenna at the sub-6 GHz band and (b) at the mm-wave band.

and profile, the simulated gain under different AMC sizes (Fig. 6(c)) verifies the uncorrelation between λ_{low} and antenna size. Fig. 7 shows the simulated E-fields of the DFFTA. Six regions in the simulated E-filed have been numbered which correspond to six key steps within the path folding process of the DFFTA. The predefined operating mechanism of the DFFTA (Fig. 7(b)) has been verified by the simulated *co-pol* and *cross-pol* E-field. A quasi-plane *co-pol* emitted E-field is finally achieved which will generate a high-gain pencil beam at the mm-wave band.

Fig. 8 shows the simulated and measured S_{11} of the proposed antenna in two operating bands. At the sub-6 GHz band, the S_{11} keeps less than −10 dB from 3.46 to 3.57 GHz with a bandwidth of 3.1%. At the mm-wave band, the S_{11} keeps less than −10 dB from 24.0 to 32.0 GHz. The deviation of the resonance points in two bands comes from the fabrication, implementation, and test errors. The normalized radiation patterns of the antenna at the sub-6 GHz band and the mm-wave band are illustrated in Fig. 9. The low band side lobe level (SLL) is lower than −16.6 dB. The *cross-pol* level is better than −21.1 dB. At the mm-wave band, the SLL is lower than −17.4 dB and the *cross-pol* level is −23.8 dB. Fig. 10 shows the realized gain of the antenna in two bands. The antenna realizes a peak gain of 17.6 dBi at 3.53 GHz with an aperture efficiency (AE) of 68.3%. The 3-dB gain bandwidth

TABLE I

Comparison Among the Proposed Antenna and Other Works

Ref. / Freq	Aperture Size (D_0)	Profile (H)	H / D_0	3-dB Gain Bandwidth	Gain (dBi)	Aperture Efficiency
[15]	λ_{low}*D/F	$\approx 0.5\lambda_{low}$	0.23	3.6%	15.5	61.0%
C/K	($F/D \approx 0.5$)			16.0%	22.4	14.0%
[16]	λ_{low}*$D/2F$	$\approx 0.5\lambda_{low}$	0.23	7.2%	15.0	63.0%
S/Ka	($F/D \approx 0.2$)			7.1%	20.4	2.0%
[17]	λ_{low}*D/F	$\approx 0.5\lambda_{low}$	0.20	6.0%	13.8	23.8%
X/Ka	($F/D \approx 0.3$)			10.7%	23.6	28.9%
[18]	λ_{low}*$3D/2F$	$\approx 0.5\lambda_{low}$	0.19	8.1%	15.5	45.0%
X/Ka	($F/D \approx 0.5$)			34.5%	23.1	25.8%
Pro.	**Given D_0**	$\boldsymbol{D_0/8}$	**0.13**	3.9%	17.6	68.3%
S/Ka	($F/D \approx 0.5$)	$\mathbf{0.33\lambda_{low}}$		18.8%	27.8	12.2%

(1) F/D is the focal length-to-diameter ratio of the antenna array.

ranges from 3.45 GHz to 3.59 GHz (3.9%). The gain bandwidth is relatively narrow since the AMC cannot provide a smoothly varied reflection phase [13]. At the mm-wave band, a peak gain of 27.8 dBi is achieved with an AE of 12.2%. The relatively low AE results from the imperfect polarization conversion and the adopted low-directivity waveguide feed antenna. The 3-dB gain bandwidth ranges from 25.5 to 30.8 GHz (18.8%). The wide-band phase modulation of the upper metasurface and the suitable F/D (0.5) of the DFFTA together realize the wide-band gain enhancement. The simulated radiation efficiency and total efficiency of the proposed antenna at 3.5 GHz are 98.7% and 95.1%. At 28 GHz, the radiation efficiency and total efficiency of the antenna are 93.2% and 91.1%. Since the antenna profile is reduced at both bands, the realized radiation efficiency and total efficiency are relatively low.

B. *Comparison among the reported antennas*

To evaluate the performance of the proposed aperture-shared antenna, the comparison among the reported antenna is listed in Table I. It can be found that the proposed antenna achieves the highest gain with the lowest profile at sub-6 GHz and mm-wave band. In addition, the proposed antenna features a more flexible design frequency in the sub-6 GHz band under a given aperture size (D_0) and profile (D_0/8). There is no restriction between the operating frequency in the sub-6 GHz band and the profile and aperture size of the proposed antenna. Although one can choose different F/D under a given D_0 to design FPCAs with different λ_{low}, this will reduce the gain bandwidth of the FTA [16], [17]. The F/D is preferred 0.5 [19]. The proposed antenna can be an attractive choice for more space-constrained 5G systems.

V. Conclusion

A low-profile aperture-shared dual-band antenna hybridizing a sub-6 GHz FPCA and an mm-wave DFFTA is detailly studied in this letter. The proposed hybridization procedure releases the restrictions between the low band operating frequency and the aperture size and profile of the aperture-shared antenna. Lower antenna profile at both working bands and more flexible design frequency at the lower band have been achieved. The proposed aperture-shared antenna can be potentially applied in the sub-6 GHz/mm-wave integrated 5G systems. The future work will lie in the dual-band aperture-shared antenna with a wide 3-dB gain bandwidth and high aperture efficiency.

References

[1] C. -X. Mao, S. Gao, Y. Wang, Q. -X. Chu and X. -X. Yang, "Dual-Band Circularly Polarized Shared-Aperture Array for C-/X-Band Satellite Communications," *IEEE Trans. Antennas Propag.*, vol. 65, no. 10, pp. 5171–5178, Oct. 2017.

[2] J. F. Zhang, Y. J. Cheng, Y. R. Ding, and C. X. Bai, "A dual-band shared-aperture antenna with large frequency ratio, high aperture reuse efficiency, and high channel isolation," *IEEE Trans. Antennas Propag.*, vol. 67, no. 2, pp. 853–860, Feb. 2019.

[3] F. Qin et al., "A simple low-cost shared-aperture dual-band dual-polarized high-gain antenna for synthetic aperture radars," *IEEE Trans. Antennas Propag.*, vol. 64, no. 7, pp. 2914–2922, Jul. 2016.

[4] D. M. Pozar and S. D. Targonski, "A shared-aperture dual-band dual-polarized microstrip array," *IEEE Trans. Antennas Propag.*, vol. 49, no. 2, pp. 150–157, Feb. 2001.

[5] C.-X. Mao, S. Gao, Q. Luo, T. Rommel, and Q.-X. Chu, "Low-cost X/Ku/Ka-band dual-polarized array with shared aperture," *IEEE Trans. Antennas Propag.*, vol. 65, no. 7, pp. 3520–3527, Jul. 2017.

[6] O. El Ayach, S. Rajagopal, S. Abu-Surra, Z. Pi, and R. W. Heath, Jr., "Spatially sparse precoding in millimeter wave MIMO systems," *IEEE Trans. Wireless Commun.*, vol. 13, no. 3, pp. 1499–1513, Mar. 2014.

[7] W. Roh et al., "Millimeter-wave beamforming as an enabling technology for 5G cellular communications: Theoretical feasibility and prototype results," *IEEE Commun. Mag.*, vol. 52, no. 2, pp. 106–113, Feb. 2014.

[8] X. Wang et al., "Millimeter wave communication: A comprehensive survey," *IEEE Commun. Surveys Tuts.*, vol. 20, no. 3, pp. 1616–1653, 3rd Quart., 2018.

[9] M. Agiwal, A. Roy, and N. Saxena, "Next generation 5G wireless networks: A comprehensive survey," *IEEE Commun. Surveys Tuts.*, vol. 18, no. 3, pp. 1617–1655, 3rd Quart., 2016.

[10] J. Zhu, Y. Yang, S. Liao, S. Li, and Q. Xue, "Dual-Band Aperture-Shared Fabry–Perot Cavity-Integrated Patch Antenna for Millimeter-Wave/Sub-6 GHz Communication Applications," *IEEE Antennas Wirel. Propag. Lett.*, vol. 21, no. 5, pp. 868–872, May. 2022.

[11] Q. Wang, Y. Mu, and J. Qi, "A Novel Reflection-Mode Fabry–Perot Cavity Antenna With Broadband High Gain and Large Beam-Scanning Angle by Janus Partially Reflective Surface," *IEEE Trans. Antennas Propag.*, vol. 71, no. 2, pp. 1350–1358, Feb. 2023.

[12] Q. Wang, J. Qi, and A. Sihvola, "A Triple-Band Uni-Cavity Fabry–Perot Cavity Antenna With Hybrid Excitation Modes," *IEEE Trans. Antennas Propag.*, vol. 71, no. 6, pp. 4851–4861, Jun. 2023.

[13] J. Qi et al., "Low-Profile Uni-Cavity High-Gain FPC Antenna Covering Entire Global 2.4 GHz and 5 GHz WiFi-Bands Using Uncorrelated Dual-Band PRS and Phase Compensation AMC," *IEEE Trans. Antennas Propag.*, vol. 70, no. 11, pp. 10187–10198, Nov. 2022.

[14] P. Mei, X. Q. Lin, G. F. Pedersen, and S. Zhang, "Design of a Triple-Band Shared-Aperture Antenna With High Figures of Merit," *IEEE Trans. Antennas Propag.*, vol. 69, no. 12, pp. 8884–8889, Dec. 2021.

[15] Z. -G. Liu, R. -J. Yin, and W. -B. Lu, "A Novel Dual-Band Shared-Aperture Antenna Based on Folded Reflectarray and Fabry–Perot Cavity," *IEEE Trans. Antennas Propag.*, vol. 70, no. 11, pp. 11177–11182, Nov. 2022.

[16] J. Zhu, Y. Yang, S. Liao, and Q. Xue, "Aperture-Shared Millimeter-Wave/Sub-6 GHz Dual-Band Antenna Hybridizing Fabry–Pérot Cavity and Fresnel Zone Plate," *IEEE Trans. Antennas Propag.*, vol. 69, no. 12, pp. 8170–8181, Dec. 2021.

[17] P. Mei, S. Zhang, and G. F. Pedersen, "A Dual-Polarized and High-Gain X-/Ka-Band Shared-Aperture Antenna With High Aperture Reuse Efficiency," *IEEE Trans. Antennas Propag.*, vol. 69, no. 3, pp. 1334–1344, Mar. 2021.

[18] S. Gao and H. Wong, "Design of a Dual-Band Shared-Aperture Antenna Combining Fabry-Perot Cavity and Folded Transmitarray for *X* and *Ka* Bands," *IEEE Trans. Antennas Propag.*, vol. 72, no. 1, pp. 323–331, Jan. 2024.

[19] T. -J. Li, G. -M. Wang, T. Cai, H. -P. Li, J. -G. Liang, and J. Lou, "Broadband Folded Transmitarray Antenna With Ultralow-Profile Based on Metasurfaces," *IEEE Trans. Antennas Propag.*, vol. 69, no. 10, pp. 7017–7022, Oct. 2021.

[20] C. Fan, W. Che, W. Yang, and S. He, "A Novel PRAMC-Based Ultralow-Profile Transmitarray Antenna by Using Ray Tracing Principle," *IEEE Trans. Antennas Propag.*, vol. 65, no. 4, pp. 1779–1787, Apr. 2017.

[21] T. -J. Li, G. -M. Wang, H. -P. Li, and H. -S. Hou, "Circularly Polarized Double-Folded Transmitarray Antenna Based on Receiver-Transmitter Metasurface," *IEEE Trans. Antennas Propag.*, vol. 70, no. 11, pp. 11161–11166, Nov. 2022.

[22] J. Zhu, Y. Yang, S. Liao, and Q. Xue, "Dual-Band Antenna Hybridizing Folded Transmitarray and Folded Reflectarray," *IEEE Trans. Antennas Propag.*, vol. 70, no. 4, pp. 3070–3075, Apr. 2022.

[23] D. Kim and J. Yeo, "Dual-Band Long-Range Passive RFID Tag Antenna Using an AMC Ground Plane," *IEEE Trans. Antennas Propag.*, vol. 60, no. 6, pp. 2620–2626, Jun. 2012.

[24] Z. Li et al., "Low-profile and wideband gain enhanced Fabry–Perot cavity antenna using gradient PRS and AMC," *IET Microwaves, Antennas & Propagation*, vol. 14, no. 15, pp. 1952–1959, Oct. 2020.

[25] G. G. Khang, S. J. Kim, and D. Kim, "High-Gain Fabry–Perot Cavity Antenna With an Artificial Magnetic Conductor Side Wall," *IEEE Antennas Wirel. Propag. Lett.*, vol. 22, no. 9, pp. 2245–2249, Sep. 2023.